coatings

Communication

Effect of High-Energy Shot Peening on Properties of High-Velocity Oxygen-Fuel Spraying

Fengbo Li [1,2,*], Conghui Zhang [1,*], Qingtao Pang [2], Gang Fang [2] and Guoqiang Xu [2]

1 School of Metallurgical Engineering, Xi'an University of Architecture and Technology, Xi'an 710055, China
2 Shaanxi Coal Chemical New Energy Technology Co., Ltd., Xi'an 710100, China
* Correspondence: coollifengbo@foxmail.com (F.L.); zhangconghui@xauat.edu.cn (C.Z.)

Abstract: A Cr_3C_2-Al_2O_3-NiCr composite coating was prepared on an INCONEL600 alloy surface through high-velocity oxygen-fuel spraying followed by further processing through high-energy shot peening to create the composite coating. The microhardness and friction properties of the composite coating are analyzed by a microhardness tester and reciprocating friction tester. The microscopic structure and wear trace of the composite coating were analyzed by scanning electron microscope (SEM). The element distribution of the coating was analyzed by energy-dispersive spectroscopy (EDS). The porosity of the coating was detected by industrial CT. The phase and residual stress of the coating were tested by X-ray diffraction (XRD). The electrochemical corrosion and friction wear performance of the samples under different surface states were discussed. The results showed that the compactness of the coating was improved and the porosity was significantly reduced after high-energy shot peening. The high-energy shot peening did not alter the phase composition of the coating but introduced residual compressive stress. The microhardness of theCr_3C_2-Al_2O_3-NiCr high-velocity oxygen-fuel coating can reach 2.9 times that of the INCONEL600 substrate, and the hardness of the coating after high-energy shot peening can reach 3.9 times of that of the substrate. After high-energy shot peening, the corrosion resistance of the coating in HCl solution is improved. Compared with the INCONEL600 substrate, the friction coefficient and calculated wear rate of the Cr_3C_2-Al_2O_3-NiCr high-velocity oxygen-fuel coating decrease by 62.5% and 79.6%, respectively. After high-energy shot peening, the friction coefficient and calculated wear rate of the coating decrease by 75% and 98.7%, respectively.

Keywords: coating; high-energy shot peening; wear; corrosion

check for updates

Citation: Li, F.; Zhang, C.; Pang, Q.; Fang, G.; Xu, G. Effect of High-Energy Shot Peening on Properties of High-Velocity Oxygen-Fuel Spraying. *Coatings* **2023**, *13*, 872. https://doi.org/10.3390/coatings13050872

Academic Editor: Philipp Vladimirovich Kiryukhantsev-Korneev

Received: 10 April 2023
Revised: 28 April 2023
Accepted: 3 May 2023
Published: 5 May 2023

1. Introduction

INCONEL600 alloy has excellent high-temperature strength, good oxidation resistance and thermal corrosion resistance; it is a high-temperature metal material suitable for long-term work above 760–1500 °C [1,2]. However, the alloy has some problems, such as low hardness and insufficient wear resistance, which limit the industrial application of the alloy. Studies have shown that INCONEL 600 alloy is prone to wear failure due to fretting wear and sliding wear [3,4]. Wear failure not only causes a lot of waste of materials and components, but may also lead to disastrous consequences. Particularly for equipment with flowing media inside, the abrasion of key parts has a great impact on the service of equipment, so it is particularly critical to strengthen the surface of the key parts of said equipment [5,6].

To improve the wear resistance of workpieces, apart from the changing of matrix materials and of workpiece structures, wear-resistant coatings are generally prepared on the surface of workpieces. Wear-resistant coatings can generally be divided into diffusion coatings and overlay coatings, such as C-diffusion coatings [7] and N-diffusion coatings [8]. Overlay coatings are formed by utilizing physical or chemical methods to directly deposit coating materials on the alloy surface. Unlike diffusion coatings, the substrate does not participate in the formation of the coating during the preparation of overlay coatings, so the selection of the coating's composition is more diverse; multiple preparation methods have also been developed, such as laser cladding [9], surface overlay welding [10], and explosion spraying [11]. Thermal spraying, as an overlaying coating making method, is a scalable and cost-efficient surface engineering method which can deposit thick coatings with a wide variety of metallic and non-metallic feedstock materials. Xiao et al. [12] applied APS to prepare NiCrBSi-Zr coating and found that it has lower porosity and excellent anti-friction and wear resistance. Ding et al. [13] used HVOF technology to prepare WC-12Co coating, and the results showed that the coating has a higher bonding strength and more excellent wear resistance.

Cr_3C_2-NiCr cermet composite coating has attracted wide attention because of its high hardness of hard phase Cr_3C_2 and high toughness of binder phase NiCr [14,15]. Many studies have analyzed the relationship between process parameters and coating microstructure and properties and discussed the failure mechanisms of the coating, such as corrosion, wear and high-temperature oxidation [16,17]. Previous studies show that the coating often has defects such as poor porosity and poor bonding with the substrate, which lead to the failure of the coating under harsh working conditions. Therefore, it is necessary to adjust the microstructure or properties of the coating using high-quality and efficient post-treatment technology. Annealing [18,19] and laser remelting [20–22] are mostly used in coating post-treatment, which improves the bonding strength, microhardness and wear resistance of the coating to a certain extent. It is challenging to completely remove the residual tensile stress on the coating surface with heat treatment [23], and this is not conducive to the long-term service of the coating. High-energy shot peening can improve the surface structure and hardness of materials, and introduce residual compressive stress to optimize the service performance of materials [24,25].

In this study, post-process shot peening was used to improve the structures and tribological properties of a cold-sprayed Cr_3C_2-Al_2O_3-NiCr coating. The influence of shot peening on phase compositions, microstructures, mechanical and corrosion properties of Cr_3C_2-Al_2O_3-NiCr coatings was investigated, respectively, and its mechanism was further discussed.

2. Materials and Methods

The substrate material is INCONEL600 alloy, manufactured by Western Superconducting Technologies Co., Ltd. (Xi'an, China) The chemical composition is listed in Table 1. Before preparing the spraying, the surface of INCONEL600 alloy was polished, degreased and sandblasted. The spraying powder is 25% Cr_3C_2 powder, 5% Al_2O_3 powder and 70% NiCr powder, which are uniformly mixed by ball mill. The spraying powder is manufactured by Xi'an Surface Material Protection Co., Ltd. (Xi'an, China).

Table 1. Chemical composition of INCONEL600 alloy.

Element	C	Mn	Si	P	S	Cr	Ni	Cu	Fe
wt.%	≤0.15	≤1.00	≤0.50	≤0.030	≤0.015	14.0–17.0	71.0–78.0	≤0.50	6.0–10.0

The spraying equipment is a KY-HVO (A) F(Xi'an, China) high-velocity spraying machine, which uses aviation kerosene as fuel, high pressure oxygen as combustion-supporting gas and nitrogen as powder feeding gas. Figure 1 explain the principle of its operation. The fuel is mixed with high-pressure oxygen and burned in a nozzle to produce a high -temperature, high-speed flame flow. The coating powder is accelerated, mixed and melted by high-speed flame flow, and finally hits the substrate surface at high speed to form the coating. The high-energy shot peening treatment was carried out using air pressure shot peening equipment (DT1480, Shanghai, China), the shot medium is a glass ball with a diameter of 0.3 mm, the working pressure is 0.2 MPa, and the shot peening time is 5 min.

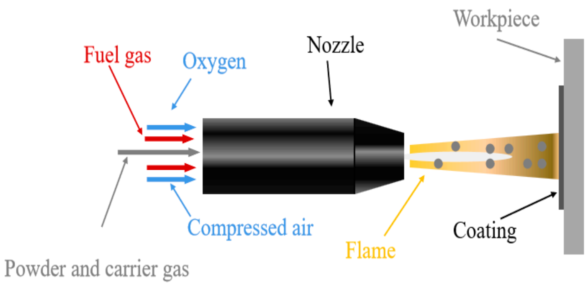

Figure 1. Schematic diagram of high-velocity spraying.

A JSM-6460 (JEOL Ltd.,Tokyo, Japan,) scanning electron microscope (with EDS) was used to observe the micro-morphology of the coating pores, and the wear marks and element distribution of the samples. An MH-5 (Shanghai Hengyi Technology Company, Shanghai, China) microhardness tester was used to measure the microhardness of the samples (loading load 5N, loading time 15 s, taking 5 points for each datum and taking the average value); a CHI800D (Shanghai Chenhua Instrument Co., Ltd., Shanghai, China) electrochemical workstation, was used to detect the Taffel curve of the samples. The scanning range was −1.0–1.0 V, and the corrosion medium was 5% HCl solution. The phases of the coatings before and after shot peening were characterized by XRD (SHIMADZU, Kyoto, Japan), with Cu-Ka radiation. The diffraction angle was in the range of 30–85°. An X-ray stress analyzer (SHIMADZU) was used to measure the surface residual stress of coating before and after shot peening with $\sin^2\psi$ method. Industrial CT (Huiyan Technology Co., Ltd., Beijing, China) was used to measure the porosity of the coating before and after shot peening.

All of the surfaces to be rubbed were uniformly polished with #1500 sandpaper. The friction time was 30 min and the load was 200 g. The wear test was conducted using an MSR-2T type reciprocating friction and wear tester, as shown in Figure 2. The upper specimen was a 6 mm diameter Al_2O_3 ball with a Vickers hardness of approximately 2035 HV and a density of 3.6 g/cm^3. The lower specimen was the test specimen, and the load was provided by the upper weight, with a test speed of 40 mm/min and a stroke of 5 mm. The dry friction test was conducted at room temperature. In the friction and wear test, the software MSR-2T (Lanzhou Zhongke Kaihua Technology Development Co., Ltd., Lanzhou, China) recorded the changing trend of the friction coefficient with time. A DSX510 (Olympus) three-dimensional profilometer was used to measure the cross-sectional area of the wear area of the material, and the wear rate was calculated using the following Formula (1):

$$W_r = \frac{W_v}{S \times L} \tag{1}$$

Wr—Rate of wear mm^3/(m·N)
Wv—Wear volume (mm^3)
S—Sliding distance (mm)
L—Load (N)

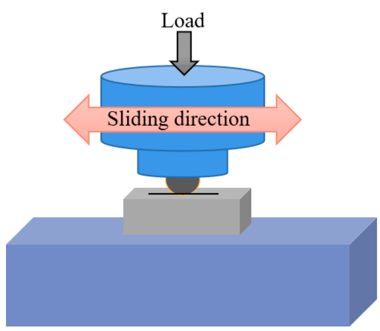

Figure 2. Schematic diagram of friction and wear experiments.

3. Results

3.1. SEM and EDS Investigation of Coating

The coating section before and after high-energy shot peening was investigated by SEM, as shown in Figure 3. Prior to investigation, all the specimens' observed surfaces were polished. It can be seen that the coating structure is loose and has many pores both before and after shot peening. Image J 1.54c software was used to mark the images before and after shot peening, with the yellow area in the figure marked as pores. Through software analysis, the average pore area on the coating before shot peening was found to be 563.642 μm^2, while after shot peening it decreased to 277.197 μm^2. This indicates that the coating was compressed and the compactness was improved after shot peening.

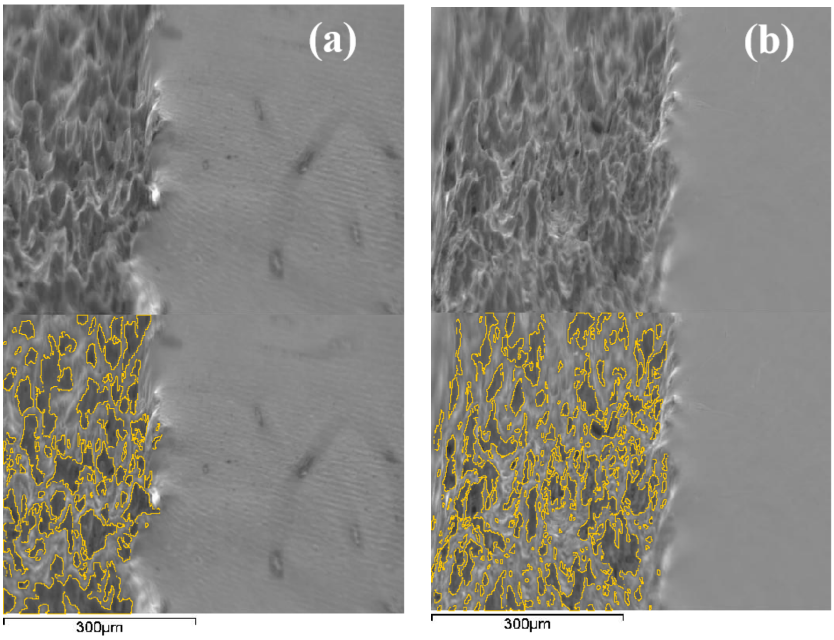

Figure 3. Cross-sectional SEM. (**a**) Coating, (**b**) Coating + peening.

The coating surface before and after shot peening was investigated by SEM and EDS, as shown in Figure 4. It can be seen that after shot peening, elements C, Cr and Ni on the coating surface are more evenly distributed than those before shot peening, and the agglomeration of elements disappears. The results indicate that the distribution of Cr_3C_2 and NiCr phases in the coating was more uniform after shot peening.

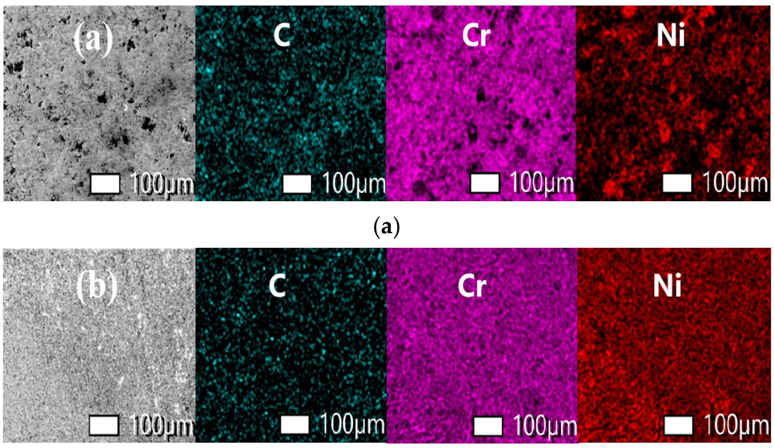

(**a**)

(**b**)

Figure 4. Surface SEM and EDS (**a**) Coating, (**b**) Coating + peening.

3.2. Porosity Analysis

In order to investigate the distribution of pores in the coating before and after shot peening, this study used industrial CT to detect the coating before and after high-energy shot peening, as shown in Figure 5. The red areas in the figure represent the pores distributed in the coating. After statistical analysis, it was found that the porosity of the coating sample was 12.68%, which decreased to 4.75% after high-energy shot peening. Porosity is an important factor affecting the corrosion resistance of the coating. Kawakita J et al. [26] found that an increase in porosity would result in reduced corrosion resistance. The above results show that the porosity of the coating can be significantly reduced by high-energy shot peening.

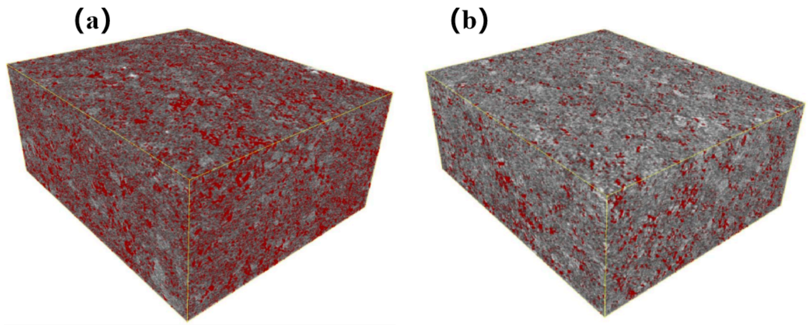

Figure 5. Porosity detection by CT (**a**) Coating, (**b**) Coating + peening.

3.3. Hardness Test

Hardness is one of the most important indices for measuring the wear resistance of materials, and the remarkable improvement of hardness can effectively improve the wear resistance of materials. Mechanical surface hardening treatments such as shot peening [27], laser shock peening [28], and rolling [29] can induce elastic-plastic deformation on the surface, and may improve the hardness of thermal sprayed coatings. In order to fully describe the coating hardness, 5 points were measured randomly for each sample. Figure 6 shows the mean microhardness test results of three samples. It can be seen that the hardness of the substrate is 172.7 ± 3.3 HV, the hardness of the coating is 497.3 ± 25.4 HV, and the hardness of the coating + shot peening sample is 674.0 ± 6.8 HV. The mean hardness of the coating reaches 2.9 times that of the substrate, and the hardness of the coating is further improved after high-energy shot peening, reaching 3.9 times that of the substrate.

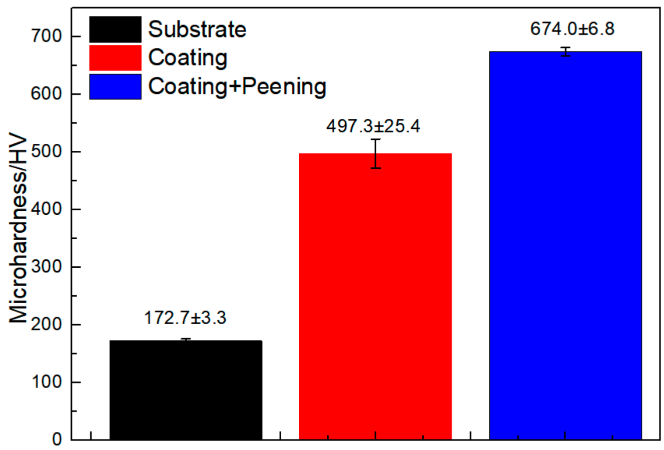

Figure 6. Results of the hardness test.

After high-energy shot peening, the standard deviation of hardness is significantly reduced, which indicates that the hardness distribution of the coating is more uniform after shot peening. It can be seen from the surface EDS results that after high-energy shot peening, the distribution of Cr_3C_2 and NiCr phases in the coating is more uniform, which is indeed due to the uniform distribution of phase leading to the uniform distribution of hardness.

3.4. XRD Phase and Residual Stress Detection

In order to study the effect of high shot peening on the phase and residual stress of coatings, the samples were tested by XRD, and Jade 6.5 software was used to mark the phase. The XRD diffractograms of the coating before and after high-energy shot peening is shown in Figure 7. It can be seen that the coating is mainly composed of NiCr phase and Cr_3C_2 phase. A small amount of Cr_7C_3 and $Cr_{23}C_6$ phases also appeared, which proved that a slight decarburization occurred during the spraying process. As can be seen in the diffractogram, no phase changed, indicating that the crystallinity of these coatings was not changed in the process of shot peening.

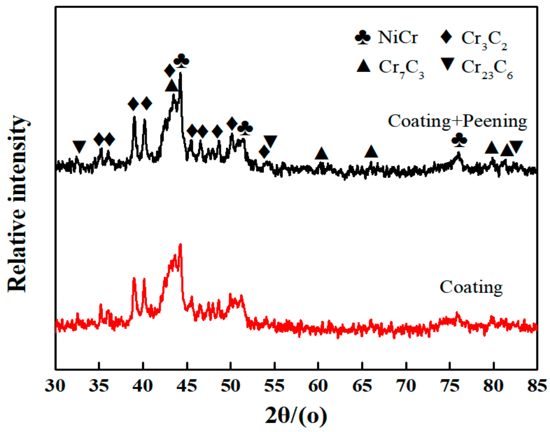

Figure 7. XRD diffraction patterns of coating and coating + peening.

Another characteristic of shot peening was the introduction of compressive residual stress. As shown in Table 2, the residual stress of the thermal-sprayed coating was found to be 15 MPa. After shot peening, the tensile residual stress was transformed into compressive stress with a value of −131 MPa. Zhao et al. found that coating corrosion resistance may be improved by optimizing the residual stress in conjunction with coating thickness and the geometry of common defects [30]. Ma et al. reported that inducing a compressive residual stress field can hinder the fatigue crack initiation and growth [31]. Therefore, the corrosion or other mechanical properties of the coating may be improved by introducing residual compressive stress after high-energy shot peening

Table 2. Residual stress results of coating before and after shot peening.

Sample	Coating	Coating + Peening
Residual stress (MPa)	15 ± 4	-131 ± 7

3.5. Electrochemical Corrosion Resistance

The electrochemical corrosion polarization curve of the coating is shown in Figure 8. The analysis showed that the self-corrosion potential of the coating sample was −0.356 V, and the self-corrosion potential of the coating + shot peening sample was −0.337 V. The self-corrosion potential can characterize the corrosion tendency of the material to a certain extent, and the more positive the potential, the smaller the corrosion tendency. The self-corrosion current density was obtained by polarization curve extrapolation, and the self-corrosion current density of the coating decreased from 3.301×10^{-4} A/cm^2 to 1.978×10^{-4} A/cm^2 after shot peening. The above results showed that the density of the coating was improved and the surface porosity was decreased after high-energy shot peening, so the corrosion tendency of the coating was reduced and the corrosion resistance was improved in the HCl environment.

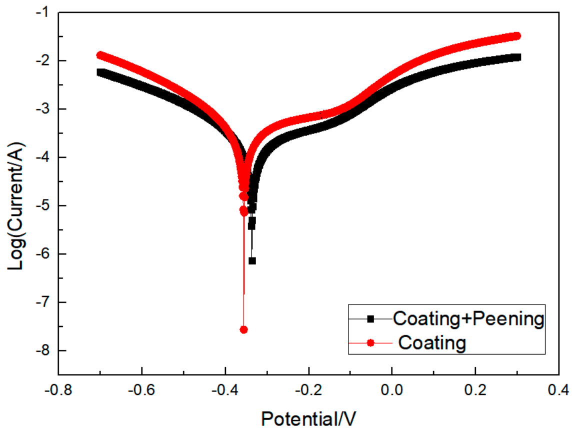

Figure 8. Taffel curve for the coating and coating + peening.

3.6. Friction and Wear Properties

The friction coefficient is a physical quantity that mainly reflects the friction state of contact surface. Figure 9 shows the friction coefficient curves of different samples and Al_2O_3 ceramic balls. It can be seen that the friction coefficient of the substrate is about 0.8, and the friction coefficient of the coating sample is about 0.3. After high-energy shot peening, the friction coefficient of the coating is further reduced to about 0.2. The results show that the surface hardness of NiCr-Cr_3C_2-Al_2O_3 coating is obviously improved after spraying on the surface of the sample, and the existence of hard particles resists the intrusion of friction pairs, which reduces the contact area between them and friction coefficient [32,33]. After high-energy shot peening, the density of the coating is improved, as well as the hardness. The ability to resist the cutting of friction pairs is stronger, and the friction coefficient is further reduced.

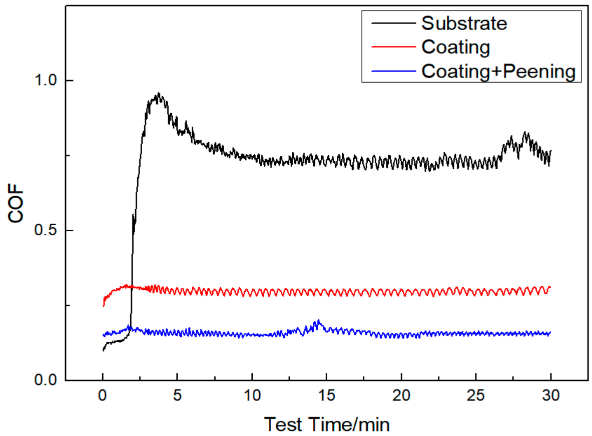

Figure 9. Curves of COF vs. test time.

In order to clarify the friction and wear properties of three different samples, the wear marks are analyzed by 3D contour scanner, and the results are shown in Figure 10a. It can be seen from the figure that a deep furrow is formed on the surface of the original sample after friction experiment, while the wear marks on the sprayed sample are very shallow. Figure 10b is the cross-sectional profile of the wear mark. After calculation, the depth of the wear mark of the original sample is 8.7 μm, and the width reaches 434.7 μm. The depth and width of the wear marks on the surface of the coating samples are 2.9 μm and 204.6 μm, which shows that the coating can effectively resist the invasion of wear balls during reciprocating friction due to the improvement of hardness, thus showing better wear resistance. After high-energy shot peening, the depth and width of the wear marks are further reduced to 0.5 μm and 104.9 μm, and the penetration depth of the wear balls is further reduced due to the continuous increase in hardness of the coating.

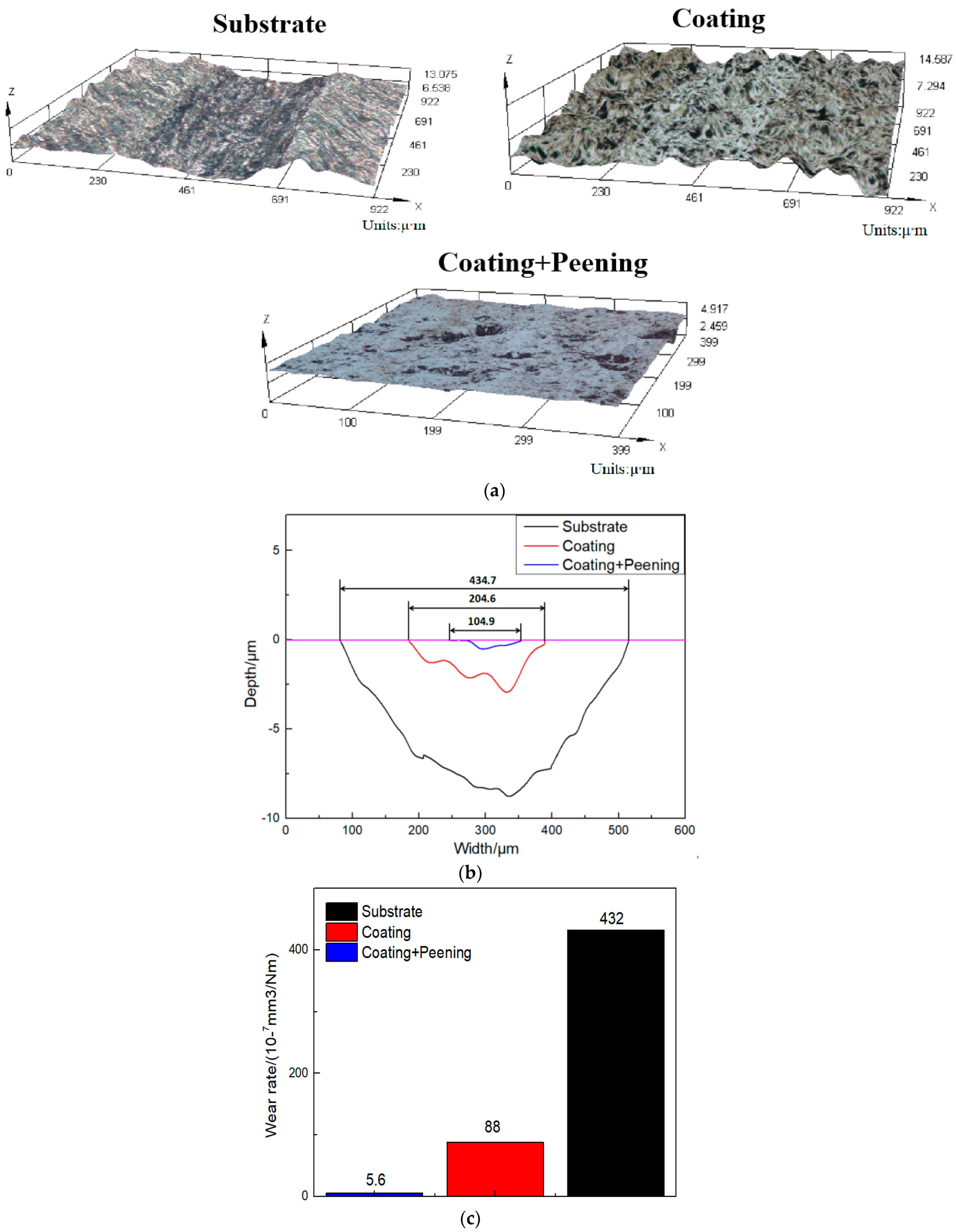

Figure 10. Friction test results: (**a**) 3D trace after friction test images. (**b**) Surface profiles of wear scar depth. (**c**) Wear rates.

Figure 10c shows the calculated wear rates of the three samples. The wear rates of the original sample are 4.32×10^{-5} mm^3/Nm, the sprayed sample is 8.8×10^{-6} mm^3/Nm, and the high-energy shot peening sample is 5.6×10^{-7} mm^3/Nm. The results show that the wear rate is reduced by 98.7% compared with the original sample through the composite treatment of spraying and high-energy shot peening, and the wear resistance is significantly improved.

4. Discussion

4.1. Morphology Analysis of Friction Marks

In order to further analyze the mechanism of improving the wear properties of the composite coating, the wear surfaces of the substrate and the composite coating are analyzed by SEM. As shown in Figure 11, deep furrows and peeling pits caused by repeated friction appear on the surface of the original sample. The friction marks on the surface of the sprayed sample are very smooth and shallow, but there are white particles on the surface of the sprayed sample after friction, and local fracture marks on the coating surface (circle area); meanwhile, the surface of the sprayed + shot peened sample has few particles, and the surface is smoother.

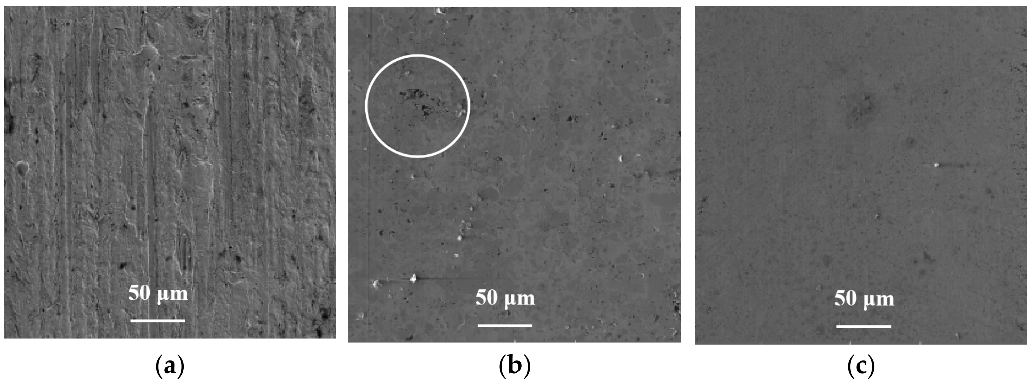

Figure 11. SEM images of substrate and coating surface after the friction experiment. (**a**) Substrate. (**b**) Coating. (**c**) Coating + peening.

It is thought that the NiCr bonding phase is easily extruded by Cr_3C_2 particles due to the plastic deformation of the surface layer at a certain depth under the action of friction during the wear process, which leads to the exposure of Cr_3C_2 particles, making it easy for them to fall off under the action of friction on the wear parts. Luo et al. [34] also reached a similar conclusion when studying the wear resistance of WC-Co coating. After high-energy shot peening, a residual compressive stress layer with a certain depth is formed on the surface of the binder. Under the action of residual compressive stress, Cr_3C_2 particles are more firmly fixed and do not fall off easily during friction. High-energy shot peening refines Cr_3C_2 particles on the surface, and the refinement of hard particles weakens the extrusion effect of the NiCr binder phase by Cr_3C_2 particles, thus avoiding excessive exposure. Therefore, high-energy shot peening can significantly improve the wear resistance of the coating.

4.2. Morphology and EDS Analysis of Friction Pair

The friction pair is tested using SEM and EDS. As shown in Figure 12, it can be seen from the friction marks on the friction pair that the friction mark width of the original sample is 230 μm, the coating sample is 110 μm wide, and the coating + shot peening sample is 80 μm wide. The narrower the width, the deeper the friction pair cuts into the substrate and the better the wear resistance. The EDS results of the friction pair surface of the original sample show that the element on the friction trace is mainly Ni, which indicates that there are elements bonded to the friction pair on the matrix. EDS results of sprayed and sprayed + shot peened samples show that the friction trace is mainly C element, the main source is hard particle Cr_3C_2, and there is no Ni or Cr element in the bonding phase. EDS results further show that the hard particle Cr_3C_2 effectively resists the friction pair cut-in, and the friction pair basically only abrades with Cr_3C_2 during the friction process; therefore, there is basically no damage to the bonding phase. The ability of the coating to resist the friction pair cut-in is further improved after high-energy shot-treatment peening.

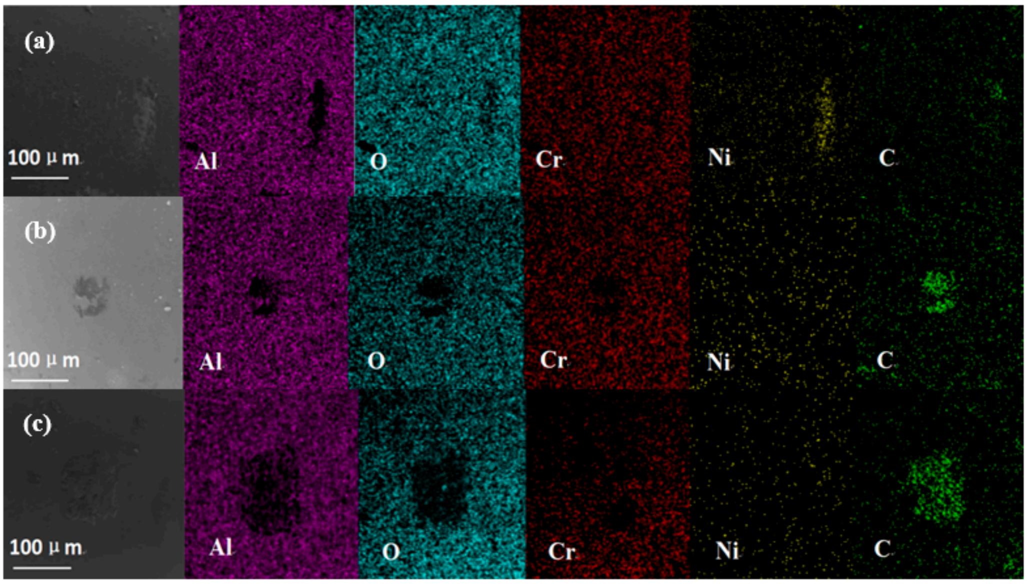

Figure 12. Surface morphology and EDS results of grinding ball corresponding to substrate and coating after the friction experiment. (**a**) Substrate. (**b**) Coating. (**c**) Coating + peening.

4.3. Stress Analysis

Figure 13 is a schematic diagram of the stress of the material during the friction process. During the grinding process between the coating sample and the friction pair, the hard particles Cr_3C_2 resist the cutting of the friction pair and avoid direct contact between the friction pair and the binder phase. The forces of the friction pair on the hard particles mainly include downward pressure N, horizontal friction f, and the binding force F around the bonding phase on hard particles. In addition to the aforementioned forces, the hard particles of the coating + high-energy shot peening samples are also affected by the residual stress δ in the binder phase. It is thought that F is the main cause of extrusion of the binder phase and the shedding of hard particles. When the force exceeds the tensile strength of binder phase, the binder phase fails.

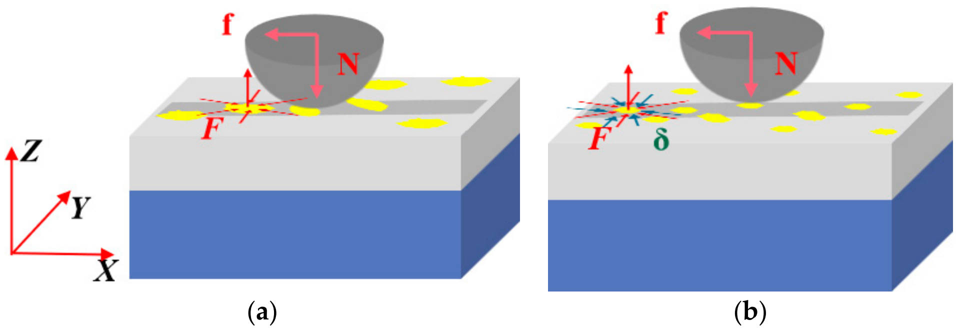

Figure 13. Schematic diagram of stress analysis of coating: (**a**) Coating, (**b**) Coating + peening.

Under the influence of residual stress δ and lower friction force f, the binding force F of the coating + high-energy shot peening samples is smaller. The friction resistance of the coating + shot peening sample surface layer is better, indicating that the friction resistance of the coating is significantly improved by high-energy shot peening.

4.4. Effect of Surface Strengthening Layer on Wear Properties

After high-energy shot peening, a strengthened layer with a certain depth is formed on the surface of the coating, and the hardness is high. Some studies have shown that there is a residual compressive stress layer with a certain depth in the coating after shot peening [35–37]. According to the Archard equation [38], the relationship between hardness (H) and wear rate (W) is shown in Equation (2):

$$W = K\frac{P}{H} \tag{2}$$

where K is the friction coefficient of materials, P is the applied load, and H is the hardness. As described in Equation (2), the wear rate w decreases with the increase in hardness (H). The existence of residual compressive stress can effectively inhibit the fatigue wear caused by periodic load at the contact point during friction [39,40], and inhibit the initiation and development of fatigue cracks in the coating.

5. Conclusions

1. After high-energy shot peening, the compactness of the coating was improved and the porosity was significantly reduced.
2. The microhardness of the Cr_3C_2-Al_2O_3-NiCr high-velocity oxygen-fuel coating can reach 2.9 times of that of the INCONEL600 substrate, and the hardness of the coating after high-energy shot peening can reach 3.9 times of that of the substrate.
3. After high-energy shot peening, the corrosion tendency of the coating was reduced and the corrosion resistance was improved in the HCl environment.
4. Compared with the INCONEL600 substrate, the friction coefficient and calculated wear rate of the Cr_3C_2-Al_2O_3-NiCr high-velocity oxygen-fuel coating decrease by 62.5% and 79.6%, respectively. After high-energy shot peening, the friction coefficient and calculated wear rate of the coating decrease by 75% and 98.7%, respectively.

Author Contributions: Experiments and writing—original draft, F.L.; Study design, F.L. and C.Z.; Supervision, Q.P. and G.X.; Writing—review and editing, G.F. All authors have read and agreed to the published version of the manuscript.

Funding: This work was supported by the National Key Research and development Program of China (Grant Nos. 2021YFB4000904).

Institutional Review Board Statement: Not applicable.

Informed Consent Statement: Not applicable.

Data Availability Statement: Data presented in this article is available upon request from the corresponding author.

Acknowledgments: Thanks to Xi'an Surface Material Protection Co., Ltd. engineers for their help in the processing of the sample for this study.

Conflicts of Interest: The authors declare no conflict of interest.

References

1. Lee, K.Y.; Hwang, C.S.; Kim, S.J.; Kim, G.G.; Kim, J.H.; Yoon, C.S. *Reciprocating Sliding Wear Behavior of Inconel 600 Mated with SUS 304 Stainless Steel at Elevated Temperatures*; Trans Tech Publications: Chengdu, China, 2006; pp. 270–273.
2. Abels, J.M.; Strehblow, A.H. A surface analytical approach to the high temperature chlorination behaviour of inconel 600 at 700 °C. *Corros. Sci.* **1997**, *39*, 115–132. [CrossRef]
3. Lim, M.K.; Oh, S.D.; Lee, Y.Z. Friction and wear of Inconel 690 and Inconel 600 for steam generator tube in room temperature water. *Nucl. Eng. Des.* **2003**, *226*, 97–105. [CrossRef]
4. Kim, H.; Choi, J.H.; Kim, J.K.; Park, K.S.; Kim, S.T.; Kim, S.J. The Sliding Wear Behavior of Inconel 600 Mated with SUS 304. *Korean J. Mater. Res.* **2001**, *11*, 841–845.
5. Wang, Q.; Chen, Z.H.; Ding, Z.X.; Liu, Z.L. Performance study of abrasive wear and erosive wear of WC-12Co coatings sprayed by HVOF. In Proceedings of the IEEE International Nanoelectronics Conference, Shanghai, China, 22–27 March 2008.

6. Zhu, J.; Lim, C.J.; Grace, J.R.; Lund, J.A. Tube wear in gas fluidized beds—II. Low velocity impact erosion and semi-empirical model for bubbling and slugging fluidized beds. *Chem. Eng. Sci.* **1991**, *46*, 1151–1156. [CrossRef]
7. Morita, T.; Hirano, Y.; Asakura, K.; Kumakiri, T.; Ikenaga, M.; Kagaya, C. Effects of plasma carburizing and DLC coating on friction-wear characteristics, mechanical properties and fatigue strength of stainless steel. *Mater. Sci. Eng. A* **2012**, *558*, 349–355. [CrossRef]
8. Fazlalipour, F.; Niki Nushari, M.; Shakib, N.; Shokuhfar, A. Comparative Tribological Behavior of V(N,C) and VC Diffusion Coatings. In *Defect & Diffusion Forum*; Trans Tech Publications: Stafa-Zurich, Switzerland, 2010.
9. Kagiyama, A.; Terakado, K.; Urao, R. Effect of nitriding and TiN coating temperatures on the corrosion resistance of the combined surface modification layer. *Surf. Coat. Technol.* **2003**, *169*, 397–400. [CrossRef]
10. Novák, P.; Müller, M.; Hrabě, P. Application of overlaying material on surface of ploughshare for increasing its service life and abrasive wear resistance. *Agron. Res.* **2015**, *13*, 158–166.
11. Tian, H.L.; Guo, M.Q.; Wang, C.L.; Tang, Z.H.; Cui, Y.J. Tribological behaviour of a self-lubricated GO/WC–12Co thermal spray coating. *Surf. Eng.* **2017**, *34*, 762–770. [CrossRef]
12. Xiao, J.K.; Wu, Y.Q.; Zhang, W.; Chen, J.; Wei, X.L.; Zhang, C. Microstructure, wear and corrosion behaviors of plasma sprayed NiCrBSi-Zr coating. *Surf. Coat. Technol.* **2019**, *360*, 172–180. [CrossRef]
13. Ding, Z.X.; Chen, W.; Wang, Q. Resistance of cavitation erosion of multimodal WC-12Co coatings sprayed by HVOF. *Trans. Nonferrous Met. Soc. China* **2011**, *21*, 2231–2236. [CrossRef]
14. Vashishtha, N.; Khatirkar, R.; Sapate, S. Tribological behaviour of HVOF sprayed WC-12Co, WC-10Co-4Cr and Cr_3C_2-25NiCr coatings. *Tribol. Int.* **2017**, *105*, 55–68. [CrossRef]
15. Murthy, J.; Venkataraman, B. Abrasive wear behaviour of WC–CoCr and Cr_3C_2–20(NiCr) deposited by HVOF and detonation spray processes. *Surf. Coat. Technol.* **2006**, *200*, 2642–2652. [CrossRef]
16. Kuruba, M.; Gaikwad, G.; Natarajan, J.; Koppad, P.G. Effect of carbon nanotubes on microhardness and adhesion strength of high-velocity oxy-fuel sprayed NiCr–Cr_3C_2 coatings. *Proc. Inst. Mech. Eng. Part L J. Mater. Des. Appl.* **2022**, *236*, 86–96.
17. Liu, J.; Wang, L.; Li, F.; Ran, X.; Peng, X. Life cycle Inventory of NiCrAl/NiCr-Cr_3C_2 Composite Coatings for Plasma Spraying Process. *Procedia Manuf.* **2020**, *43*, 559–566. [CrossRef]
18. Shen, Z.; Liu, G.; Mu, R.; Yang, W.; Huang, G. The effect of vacuum heat treatment on microstructure, Al diffusion and thermal cycling lifetime of yttria stabilized zirconia by EB-PVD. *Appl. Surf. Sci. Adv.* **2021**, *4*, 100080. [CrossRef]
19. Zheng, J.; Yang, D.; Gao, Y. Effect of Vacuum Heat Treatment on the High-Temperature Oxidation Resistance of NiCrAlY Coating. *Coatings* **2020**, *10*, 1089. [CrossRef]
20. Sheng, T.; Kong, D. Wear behaviors of HVOF sprayed WC-12Co coatings by laser remelting under lubricated condition. *Opt. Laser Technol.* **2017**, *89*, 86–91.
21. Panziera, R.C.; de Oliveira, A.C.C.; Pereira, M.; Ratszunei, F. Study of the effects of the laser remelting process on the microstructure and properties of the WC–10Co–4Cr coating sprayed by HVOF. *J. Braz. Soc. Mech. Sci. Eng.* **2020**, *42*, 119. [CrossRef]
22. Mateos, J.; Cuetos, J.M.; Fernandez, E.; Vijande, R. Tribological behaviour of plasma-sprayed WC coatings with and without laser remelting. *Wear* **2000**, *239*, 274–281. [CrossRef]
23. Yang, Y.; Zhao, S.; Gong, J.; Jiang, X.; Sun, C. Effect of Heat Treatment on the Microstructure and Residual Stresses in (Ti,Al)N Films. *J. Mater. Sci. Technol.* **2011**, *27*, 385–392. [CrossRef]
24. Fard, S.B.; Guagliano, M. Effects of surfaces nanocrystallization induced by shot peening on material properties: A Review. *Frat. Integrità Strutt.* **2009**, *3*, 3–16. [CrossRef]
25. Lu, F.F.; Ma, K.; Li, C.X.; Yasir, M.; Luo, X.T.; Li, C.J. Enhanced corrosion resistance of cold-sprayed and shot-peened aluminum coatings on LA43M magnesium alloy. *Surf. Coat. Technol.* **2020**, *394*, 125865. [CrossRef]
26. Kawakita, J.; Kuroda, S.; Kodama, T. Evaluation of through-porosity of HVOF sprayed coating. *Surf. Coat. Technol.* **2003**, *166*, 17–23. [CrossRef]
27. Yao, H.-L.; Hu, X.-Z.; Yi, Z.-H.; Xia, J.; Tu, X.-Y.; Li, S.-B.; Yu, B.; Zhang, M.-X.; Bai, X.-B.; Chen, Q.-Y.; et al. Microstructure and Improved Anti-corrosion Properties of Cold-sprayed Zn Coatings Fabricated by Post Shot-peening Process. *Surf. Coat. Technol* **2021**, *422*, 127557. [CrossRef]
28. Chukwuike, V.I.; Echem, O.G.; Prabhakaran, S.; AnandKumar, S.; Barik, R.C. Laser shock peening (LSP): Electrochemical and hydrodynamic investigation of corrosion protection pre-treatment for a copper surface in 3.5% NaCl medium. *Corros. Sci.* **2020**, *179*, 109156. [CrossRef]
29. Sheng, L.Y.; Yang, F.; Xi, T.F.; Lai, C.; Ye, H.Q. Influence of heat treatment on interface of Cu/Al bimetal composite fabricated by cold rolling. *Compos. Part B Eng.* **2011**, *42*, 1468–1473. [CrossRef]
30. Zhao, X.; Munroe, P.; Habibi, D.; Xie, Z. Roles of compressive residual stress in enhancing the corrosion resistance of nano nitride composite coatings on steel. *J. Asian Ceram. Soc.* **2013**, *1*, 86–94. [CrossRef]
31. Ma, A.; Liu, D.; Zhang, X.; Liu, Y.; Zhao, W.; Wang, R.; He, G. Improving Fatigue Performance of TiZrN/TiZr-Coated Ti-6Al-4V Alloy by Inducing a Stabile Compressive Residual Stress Field. *J. Alloys Compd.* **2022**, *925*, 16679. [CrossRef]
32. Roy, M.; Venkataraman, B.; Bhanuprasad, V.V.; Mahajan, Y.R.; Sundararajan, G. The effect of participate reinforcement on the sliding wear behavior of aluminum matrix composites. *Metall. Trans. A* **1992**, *23*, 2833–2847. [CrossRef]
33. Garcia, I.; Fransaer, J.; Celis, J.P. Electrodeposition and sliding wear resistance of nickel composite coatings containing micron and submicron SiC particles. *Surf. Coat. Technol.* **2001**, *148*, 171–178. [CrossRef]

34. Luo, X.; Hong, Y.; Wu, J.; Li, S.; Yang, Q. Effect of WC Grain Size of Ultrafine WC-Co Cemented Carbide on its Friction and Wear Properities. *Rare Met. Cem. Carbides* **2022**, *050*, 93–97.
35. Du, D.; Liu, D.; Zhang, X.; Tang, J.; Meng, B. Effects of WC-17Co Coating Combined with Shot Peening Treatment on Fatigue Behaviors of TC21 Titanium Alloy. *Materials* **2016**, *9*, 865. [CrossRef] [PubMed]
36. Yuan, H.; Yao, Z.Q.; Min, Q.I. The effect of high-energy shot peening commercial pure titanium on hydroxyapatite coating by mineralization. *J. Funct. Mater.* **2007**, *38*, 1345.
37. Zhou, Z.; Shang, J.; Chen, Y.; Liang, X.; Shen, B.; Zhang, Z. Synchronous Shot Peening Applied on HVOF for Improvement on Wear Resistance of Fe-based Amorphous Coating. *Coatings* **2020**, *10*, 107. [CrossRef]
38. Farhat, Z.N.; Ding, Y.; Northwood, D.O.; Alpas, A.T. Effect of grain size on friction and wear of nanocrystalline aluminum. *Mater. Sci. Eng. A* **1996**, *206*, 302–313. [CrossRef]
39. Gao, Y.B.; Li, X.Y.; Kitchen, M.; Ding, Y.T.; Luo, Q.S. Formation mechanism and wear behavior of gradient nanostructured Inconel 625 alloy. *Trans. Nonferrous Met. Soc. China* **2022**, *32*, 1910–1925. [CrossRef]
40. Chao, L.Y.; Lakshminarayanan, R.; Shetty, D.K.; Cutler, R.A. Rolling-Contact Fatigue and Wear of CVD-SiC with Residual Surface Compression. *J. Am. Ceram. Soc.* **2010**, *78*, 2307–2313. [CrossRef]